NISTIR 7265

Effect of continued hydration on the transport properties of cracks through portland cement pastes in a saturated environment: A microstructural model study

K.A. Snyder
Jeffrey W. Bullard

National Institute of Standards and Technology
Technology Administration, U.S. Department of Commerce

NISTIR 7265

Effect of continued hydration on the transport properties of cracks through portland cement pastes in a saturated environment: A microstructural model study

K.A. Snyder
Jeffrey W. Bullard

Materials and Construction Research Division
Building and Fire Research Laboratory

Sponsor:
U.S. Nuclear Regulatory Commission

August 2005

U.S. DEPARTMENT OF COMMERCE
Carlos M. Gutierrez, Secretary

TECHNOLOGY ADMINISTRATION
Michelle O'Neill, Acting Under Secretary of Commerce for Technology

NATIONAL INSTITUTE OF STANDARDS AND TECHNOLOGY
William Jeffrey, Director

Abstract

The contribution of continued hydration to the healing of cracks in cement paste is studied using the CEMHYD3D microstructural model. After an initial period of hydration, the computational domain was divided equally into two halves, separated by water-filled elements, representing a crack, and then hydration continued. The transport factor of the composite was calculated at various intervals, from which the crack properties were calculated. The crack transport factor was a unique function of crack porosity, regardless of crack width or cement paste water:cement mass ratio. Minimum crack porosity at long times depended strongly on the fraction of unhydrated clinker when the crack was formed. For late-age cracking, the initial rate of crack filling depended upon the amount of unhydrated clinker exposed by the creation of the crack. In all cases, the majority of solids in the crack were formed by the redistribution of hydration products from the paste adjacent to the crack.

Keywords: autogeneous healing; building materials; cement paste; concrete; cracking; hydration; service life.

Contents

List of Tables

List of Figures

1 Introduction

The service performance of concrete can be influenced greatly by the presence of cracks. Therefore, long-term performance prediction for existing concrete structures containing cracks must consider the time-dependent crack transport properties. The mechanisms by which crack transport properties can change have been enumerated and classified [1–3]. In general, the mechanisms act to reduce the crack transport coefficient, effectively healing the crack.

The majority of mechanisms attributed to crack healing involve the transport of environmental material through the crack and the accumulation of reaction products within the crack. These materials may include fine particulates or calcium carbonate [4]. When these mechanisms operate, the time-dependent crack transport coefficient is a strong function of the boundary conditions. Therefore, under these circumstances, assessment of the time-dependent behavior for a particular structure can only be made if detailed knowledge of the corresponding initial and boundary conditions is available.

Another mechanism for crack healing is the formation of material from continued hydration [4, 5]. Fortunately, this particular healing mechanism can be isolated, in large part, from a particular environment. Moreover, the behavior of the system can be determined from the state of the cement paste at the time the crack occurred.

A study of crack healing by continued hydration alone has application to situations where there is brief water transport at the time of cracking, after which there is no additional convective flow. Some of these scenarios include water pipes with cementitious liners, tanks, and young concrete that has cracked because of vibration or shock. [6] The most common scenario would be healing between freezing cycles in a saturated environment [7–10]. It has been observed that continued hydration after freeze/thaw testing has led to partial or complete recovery of the ultrasonic pulse velocity [9, 11]. In one experiment, continued hydration was attributed to the *increase* in shear modulus in samples exposed to freezing and thawing after only 3 d hydration [12].

The present study focuses on continued hydration as a mechanism for crack healing, thereby reducing the number of experimental parameters. For the scenario considered, two important parameters are the initial crack volume and the volume of hydration products that fill the crack. The initial crack volume can be parameterized by the crack width. The volume of hydration product will depend on the cement paste water:cement mass ratio (w/c) and the degree of hydration at the time of cracking. If more material can be produced after cracking, the ultimate crack porosity will be lower.

Although crack width and degree of hydration are well defined laboratory experimental parameters, a computational model is used here in favor of laboratory experiments for several reasons. First, one objective of this study is to determine the crack transport properties as a function of time. Although one could make bulk conductivity and permeability measurements, a means would still be needed to unambiguously extract the crack geometry, which has been shown to have a varying width [13]. Second, the crack porosity is an important parameter, but is a time-consuming quantity to determine experimentally. A model allows one to eliminate as much of these laboratory complications as is possible. Moreover, a model study can facilitate a parametric study of principal components. This is all that is needed to learn about general behavior that is applicable

to other systems.

The NIST microstructural development model CEMHYD3D [14] is used here to perform a parametric study of the factors influencing the rate of crack healing due to continued hydration. The hydration model has been developed to accurately represent developing cement paste microstructure at the micrometer length scale, and the digital image approach facilitates the addition of planar cracks. Moreover, the CEMHYD3D model is able to mimic cement paste hydration rate [15] and cement paste formation factor [16]. These two factors alone are sufficient for capturing the salient features of crack healing.

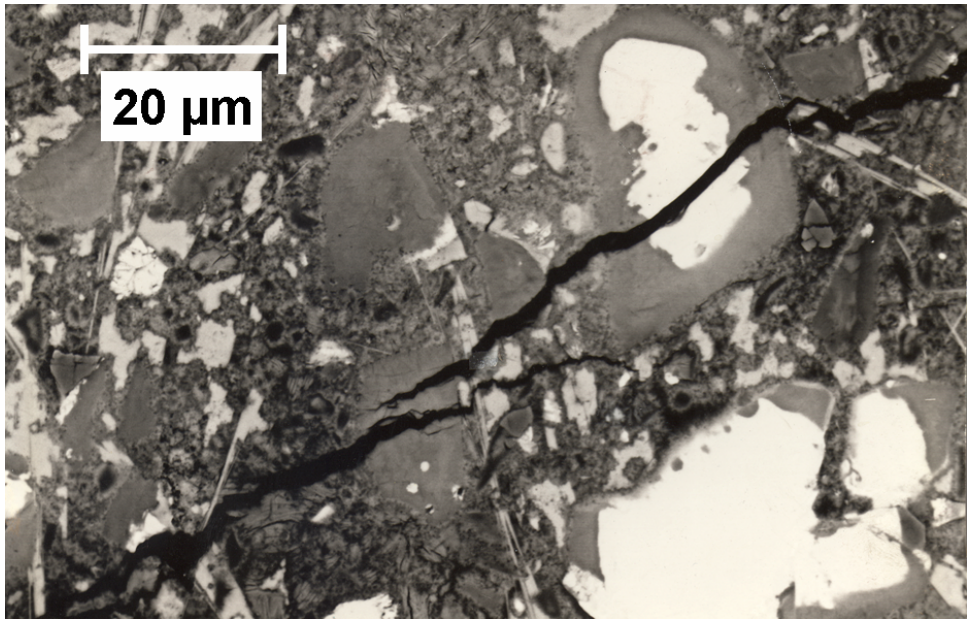

Figure 1: SEM micrograph of crack through w/c=0.45 cement paste after 28 d hydration.

The creation of cracks with smooth walls is not an unreasonable approximation for cracks in cement paste. Figure 1 shows a scanning electron microscope (SEM) micrograph of a crack propagating through a w/c=0.45 cement paste that is approximately 28 d old. The crack was generated by a microhardness tester that impacted the sample out of the field of view. The figure shows that cracks in paste can propagate in reasonably straight lines, easily passing through hydrated and unhydrated cement with minimal deviation. This evidence is meant only to justify the use of straight cracks having smooth walls in this initial study, not as a proof that all cracks are smooth and straight.

For this study, the CEMHYD3D model was modified to accommodate the addition of cracks during hydration. The initial systems were cement paste cubes having 200 μm long edges, composed of cubic voxel elements having 1 μm long edges. A crack of a given width was created by dividing the microstructure into two halves and then displacing the halves perpendicular to the dividing plane. Intervening elements were filled with water and hydration continued as before. Periodically, the microstructure was stored as an image file and the crack porosity and transport properties were calculated from the image file.

2 Crack Transport Properties

There are two crack transport properties of practical concern: diffusivity and permeability. The majority of reported studies on the effect of cracks on bulk transport have addressed permeability, [1, 4, 5, 17–22] and comparatively few have addressed diffusion/migration [23–25]. The difference in interest is somewhat proportional to the effect of cracks on each transport property.

Generally, the contribution of cracks to overall transport is the product of the crack transport property and the area fraction of cracks. In the absence of severe cracking, the area fraction of cracks is typically expressed in fractions of a percent. Given that the effective diffusivity of concrete is typically a factor of 10^{-2} smaller than that for bulk fluid in a crack, the contribution of cracks to overall diffusive transport is usually small.

By contrast, the permeability of a crack has a quadratic dependence on the crack width. As a result, the permeability of a crack could easily be one million times greater than that of the bulk concrete. Even after factoring in the crack area fraction, the crack can still contribute significantly to overall permeability.

2.1 Formation Factor

The formation factor F is a dimensionless number that characterizes the solid microstructure of a random porous media and can be related to the bulk diffusivity and permeability. For a porous solid saturated with a conducting brine, the formation factor F can be approximated by the ratio of the pore solution conductivity σ_s to the bulk (solid plus solution) conductivity σ_b:

$$F = \frac{\sigma_s}{\sigma_b} \tag{1}$$

For a nonconducting solid, this number is strictly greater than or equal to one.

For concrete, the formation factor can be used to characterize either the uncracked microstructure, the bulk cracked composite, or the crack itself. Generally, laboratory techniques probe the bulk material (cracked or uncracked) but not the crack itself. In this paper, however, the formation factor of the crack is expressed independently of the paste. This will be shown to be an important distinction that leads to greater insight into the results.

2.2 Transport Factor

A random material can be characterized either by a resistive quantity (analogous to formation factor) or by a conductive quantity, its inverse. Although either can characterize a material, in the case of transport, it seems more natural to consider the *relative* contribution to overall transport, which corresponds to the conductivity analogy. Such a quantity has been used in hydrogeological research [26], and has also been referred to as the formation factor. Here, for clarity, the conductivity analog is referred to as the transport factor L:

$$L = \frac{1}{F} \tag{2}$$

2.2.1 Influence on Diffusion

The transport factor is an important parameter for modeling diffusion in porous materials filled with electrolyte [27, 28]. Specifically, it is the parameter that relates electrolyte transport coefficients to bulk transport coefficients. Changes in the transport factor correspond to a proportional change in the effective diffusion coefficient of a particular ionic species. Therefore, changes in *crack* transport factor would correspond to proportional changes in overall bulk diffusivity, with the crack surface area being the coefficient of proportionality.

2.2.2 Influence on Permeability

The relationship between transport factor and permeability is not as direct as that for diffusivity. The difficulty arises because permeability depends upon the characteristic microstructural pore size. The Katz-Thompson [29, 30] (KT) equation, developed for geophysical research, relates permeability k to the transport factor L:

$$k = \frac{d_c^2 \, L}{\epsilon} \tag{3}$$

The quantity d_c is the microstructural critical pore diameter, and can be estimated from mercury intrusion porosimetry [29]; it is analogous to the largest diameter sphere that can pass through the microstructure. The variable ϵ is an empirical constant for a particular material: e.g., limestone, sandstone, cement paste, etc.

The KT equation can be adapted to the study of cracks by considering the relevant geometrical parameters. Using purely dimensional arguments, the critical pore diameter d_c within a crack should be a function of the crack width w and the crack porosity θ:

$$d_c = \theta^n w \tag{4}$$

Based on the work of Martys and Garboczi [31] on two-dimensional systems, the exponent n should be approximately equal to 2 for narrow cracks. If the cracks are considerably wider than the size of the particles filling the crack, the crack microstructure will be three-dimensional, and the critical pore diameter will be larger than that for a two-dimensional system at the same porosity.

For flat walls separated by a distance w, the permeability k_c of a crack with no interior solids can be calculated assuming Poiseuille flow [32]:

$$k_c = \frac{w^2}{12} \tag{5}$$

Substituting Eqn. 4 into Eqn. 3, and exploiting the exact result in Eqn. 5 in the limit $\theta, L \to 1$, yields a reasonable value of ϵ in Eqn. 3:

$$k_c = \frac{\theta^4 \, w^2 \, L}{12} \tag{6}$$

This relation is used as a starting point for estimating the permeability of healing cracks as a function of the initial crack width and the crack porosity.

Laboratory permeability measurements of cement pastes yield a w^2 dependence in the permeability, but the constant ϵ is typically greater than 12. This difference is usually attributed to crack wall surface roughness, and Eqn. 6 is multiplied by a dimensionless roughness parameter having a value between 0 and 1 [4].

3 Bulk Properties

When studying the effect of cracks on the transport properties of a concrete, it is important to distinguish between the crack transport properties and the bulk transport properties. Published experiments have determined the transport properties of a slice taken from a cylinder [19, 20, 22], in which a crack is generated using the split cylinder test. The bulk transport properties of the sample are determined as a function of the experimental parameters.

When total flow is measured in the direction along the crack, the total bulk permeability k_T is a weighted sum of the crack permeability k_c and the concrete permeability $k_\circ$:

$$k_T = \frac{A_c k_c + A_\circ k_\circ}{A_T} \tag{7}$$

The weighting factors are the crack cross-sectional area A_c, the concrete cross-sectional area $A_\circ$, and the total cross-sectional area $A_T = A_c + A_\circ$. For example, a sample taken from a 100 mm diameter cylinder would have a total cross sectional area of 7,854 mm^2. A 100 μm wide crack that spans the sample diameter will have an area of 10 mm^2 and (from Eqn. 5) a permeability k_c of 833 μm^2. Assuming a typical concrete permeability $k_\circ$ of 10 nm^2 [33], the total bulk permeability k_T is approximately 1 μm^2, a factor of 10^5 greater than the intact permeability $k_\circ$.

Although bulk permeability depends strongly on the presence of cracks, bulk permeability alone is not a sensitive measure of crack permeability. To see why, consider the previous 100 μm crack. The effect of healing on the total bulk permeability k_T can be expressed relative to the intact permeability $k_\circ$:

$$\frac{k_T}{k_\circ} \approx 1 + \frac{A_c k_c}{A_T k_\circ} \tag{8}$$

If, as the crack heals, the *bulk* permeability k_T decreases to within a factor of 2 of $k_\circ$, the *crack* permeability k_c would still be nearly a factor of 800 times greater than the concrete permeability $k_\circ$.

The use of bulk measurements to probe crack *diffusivity* is even more problematic than for crack permeability. A fresh crack has, by definition, a transport factor of one. Given a cement paste transport factor of 0.002, the bulk diffusivity would never be greater than twice the value for intact paste for the scenario given above. Generally, the transport factor of concrete would be greater, and the contribution of cracks would be more difficult to detect.

Because bulk transport properties are not sensitive indicators of the transport properties of cracks, a means is needed to determine crack properties directly. To achieve this experimentally, one must know precisely the area fraction of the crack and the transport

properties of the intact material. In addition, dissolution of mineral phases within the paste and subsequent diffusion and precipitation within the crack will alter the original paste transport properties. An account of this effect must be made because, as noted already, the corresponding changes in bulk transport coefficients are very small.

4 Crack Transport Factor

In this computational experiment, the bulk transport factor is calculated from the three-dimensional digitized microstructure image file created by CEMHYD3D. A unit electrical field is applied in each cartesian direction, and the total current in each direction is used to calculate the bulk transport factor in each of the three directions. Only water-filled porosity and calcium silicate hydrate (C-S-H) [34] are assumed to contribute to the overall conduction. The transport factor used for these two phases are as follows: water: 1.000; C-S-H: 0.005.

The crack porosity and transport factor must be calculated for each system considered. Because the crack location within the microstructure is known, the porosity of the crack is calculated from the number of saturated porosity pixels remaining in the original crack volume. The crack transport factor, however, can only be calculated indirectly. One cannot simply extract the crack microstructure from the overall microstructure and calculate the transport coefficient because the crack walls are porous and these pore play a role in transport through the crack. Instead, one would have to also extract a portion of the paste adjacent to the crack. Fortunately, there is an easier approach.

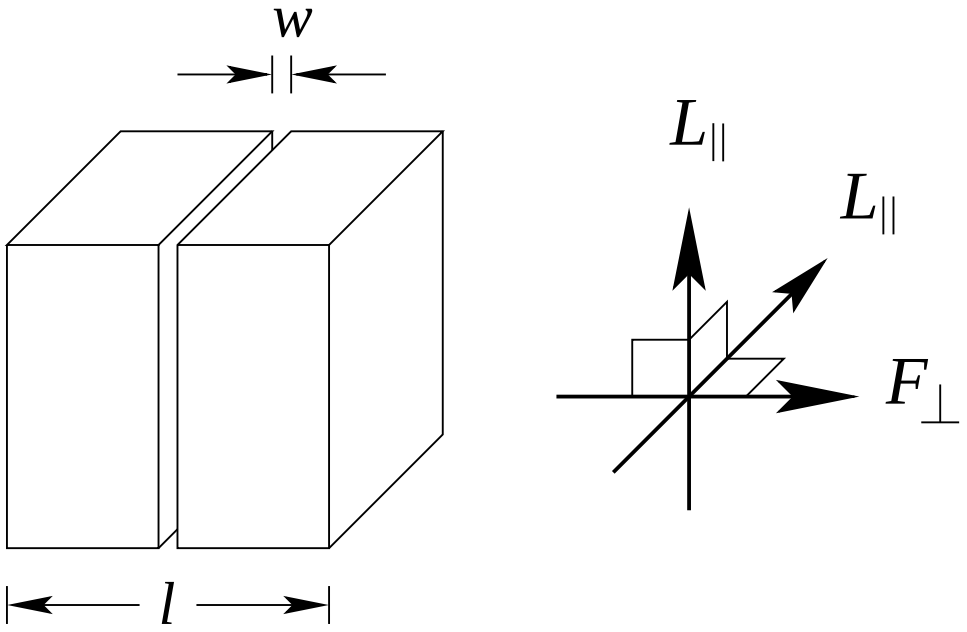

Figure 2: Schematic for the three transport coefficients calculated for each microstructure. There are three calculated coefficients: two parallel with the crack ($F_{\parallel}$), and one orthogonal to the crack ($F_{\perp}$).

The transport factor of the paste and crack are calculated from the bulk transport

factor by exploiting the symmetry of the problem. A schematic of the calculation is shown in Fig. 2, where a microstructure has been divided in two and separated by a width w that corresponds to the crack. The new width of the system is l. The conductivity calculation yields three bulk transport coefficients: two that are parallel to the crack ($L_\parallel$), and one that is perpendicular to the crack ($F_\perp$).

Due to the symmetry of the problem, the CEMHYD3D conductivity calculations in each direction can be approximated by a corresponding one-dimensional problem composed of two materials (paste and crack), each having homogeneous properties. Parallel to the crack, the contributions to the bulk *transport* factor $L_\parallel$ are in proportion to the respective lengths, and perpendicular to the crack, the contributions to the bulk *formation* factor $F_\perp$ are in proportion to the respective lengths:

$$\begin{aligned} L_\parallel &= \frac{l-w}{l} L_p + \frac{w}{l} L_c \\ F_\perp &= \frac{l-w}{l} F_p + \frac{w}{l} F_c \end{aligned} \tag{9}$$

The three measured quantities are the two values for $L_\parallel$ and one value for $F_\perp$. The subscripts p and c represent paste and crack properties, respectively. These equations were solved twice, once for each value of $L_\parallel$; the quantity $F_\perp$ was the same in both calculations. The two solutions yield four values: two values each for L_c and L_p. Because the two values for L_p were typically within 0.001 % of one another, the three reported values were the two values for L_c and one of the values for L_p.

5 CEMHYD3D

5.1 Model Description

The principles and underlying assumptions of CEMHYD3D have been described in detail elsewhere [14, 15], so only a brief summary is provided here. CEMHYD3D is a three-dimensional cellular automaton model, in which the cement paste microstructure is discretized onto a uniform cubic mesh. Each element of the mesh is filled with some material (water-filled porosity, alite, etc.). The chemical reactions comprising hydration are simulated by allowing the elements to interact according to rules that depend on the materials involved in the interaction. These rules are used to mimic dissolution of solids, diffusion of dissolved species according to a random walk algorithm, and nucleation and growth of hydration products such as portlandite and C-S-H gel. Hydration proceeds in repeated discrete cycles of dissolution, diffusion, and reaction. The elapsed time t is assumed to depend on the number n of computational cycles executed according to $t = \beta n^2$, with a scaling factor β that depends on the cement being simulated. A wide range of properties can be monitored as hydration proceeds, including heat of hydration, phase volume fractions, chemical shrinkage, percolation of capillary porosity, and setting time. Moreover, the microstructure at any time can be input to an auxiliary program to calculate its transport factor. The model has been applied with considerable success to elucidate the influence of microstructural and environmental factors on hydration kinetics and microstructure development [35–39].

5.2 Cement Characterization

Because it operates directly on cement paste microstructures, a detailed characterization of the cement powder is essential for providing accurate input to CEMHYD3D. The data required by CEMHYD3D are the cement particle size distribution (PSD), the volume fraction and surface area fraction of each cement phase and, because clinker particles are composed of multiple phases, the statistical spatial distribution of the clinker phases.

In this study a representative Type I cement was selected. The cement was issued as Cement 116 by the ASTM-sponsored Cement and Concrete Reference Laboratory (CCRL), located at the National Institute of Standards and Technology (NIST), as part of its proficiency sample program [40]. The characterization data for the cement, and a description of the methods used to obtain the data, have been published elsewhere [15].

5.3 Model Paste Formulation and Hydration

Three-dimensional, digitized microstructures of cement paste, suitable for input to the CEMHYD3D hydration model, were created using the characterization data for Cement 116. The mesh was 200 elements in each cartesian direction, for a total of 8×10^6 elements. Non-overlapping digitized spherical particles, with sizes following the measured PSD, were mapped randomly onto the mesh and the interparticle porosity was filled with water. The total volume of particles was constrained to achieve water:cement mass ratios of 0.3, 0.4, or 0.5, assuming a density of 3200 kg/m^3.

Each microstructure was input to the hydration model, and hydration was simulated at a constant temperature of 25 °C. The paste was assumed to be in contact with a reservoir of water to replenish water in the capillary pore space consumed by hydration (until the capillary pore space network became disconnected). Any crack formed during hydration also was filled with water from the reservoir.

At selected times during hydration, the hydrated microstructure was saved and the transport factor of the crack and of the bulk paste were calculated using a separate finite difference program that was designed specifically to operate on digitized microstructures [41].

6 Uncracked Paste Properties

The properties of the uncracked paste, such as degree of hydration, capillary porosity, and transport factor are presented before the results from the cracking experiment. This is done to form a point of reference for the data from the cracked pastes. In addition, the data from the uncracked systems are used to motivate the search for universal relationships between bulk and microstructural properties.

6.1 Degree of Hydration

During numerical hydration, the degree of hydration is calculated from the number of cement elements consumed by reaction. The uncracked paste degree of hydration α_p was compared to laboratory measurements based on loss-on-ignition (LOI) [15, 42], and the

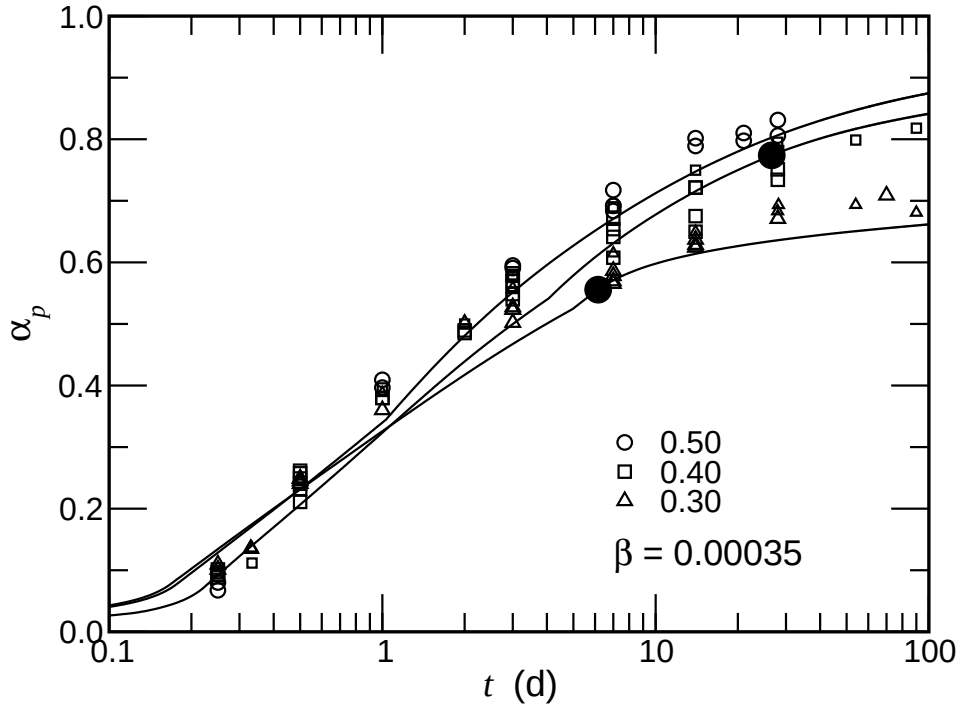

Figure 3: Paste degree of hydration α_p as a function of time t for CCRL Cement 116. Experimental results are shown as open symbols and the CEMHYD3D calculation as a solid line. Large filled circles denote the point when the capillary pores are no longer percolated.

results are shown in Fig. 3 for all three w/c values. In the figure, laboratory data are denoted by open symbols, and the values of α_p calculated by CEMHYD3D are denoted by solid curves. The calculated values were adjusted using a constant time parameter ($\beta = 0.00035$) that gave the best agreement between calculated and laboratory values.

6.2 Capillary Pore Percolation

Table 1: Approximate age (days), and corresponding degree of hydration α_p, when paste capillary porosity is no longer percolated.

	w/c	
	0.30	0.40
Age(d)	6.2	26.6
α_p	0.56	0.77

As the systems hydrate, the capillary pore space becomes filled with hydration products. For a discrete model such as CEMHYD3D, the time at which the capillary pores no

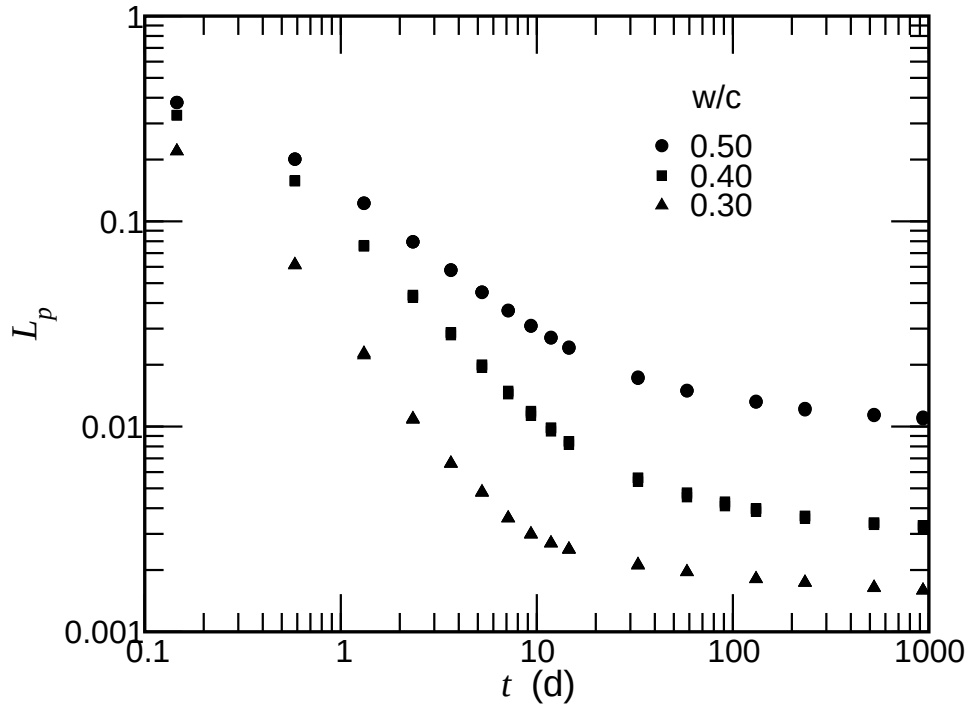

Figure 4: Paste transport factor L_p as a function of time t for the three w/c values hydrated under saturated conditions.

longer percolate can be determined uniquely. The point at which this occurs is denoted by a large filled circle in Fig. 3 for the 0.30 w/c and the 0.40 w/c pastes; the capillary pores of the 0.50 w/c paste remain percolated indefinitely. The approximate age and corresponding degree of hydration at which the capillary pores are no longer percolated are given in Table 1.

6.3 Transport Factor

The time dependence of the cement paste transport factor L_p is shown in Fig. 4 for all three w/c values. Although the time dependence of the transport factor was qualitatively similar for all three w/c values, Fig. 5 shows that more universal behavior is revealed if the data are plotted as a function of the saturated paste capillary porosity θ_p. This also has been done previously with a measure of success [16]. Here, in addition, the transport factor is scaled by its initial value $L_\circ$. It is interesting to note that when the data are presented in this manner, there is no sharp transition in the transport factor as the porosity falls below 0.20, the point at which it is assumed the capillary pores are no longer percolated [43, 44].

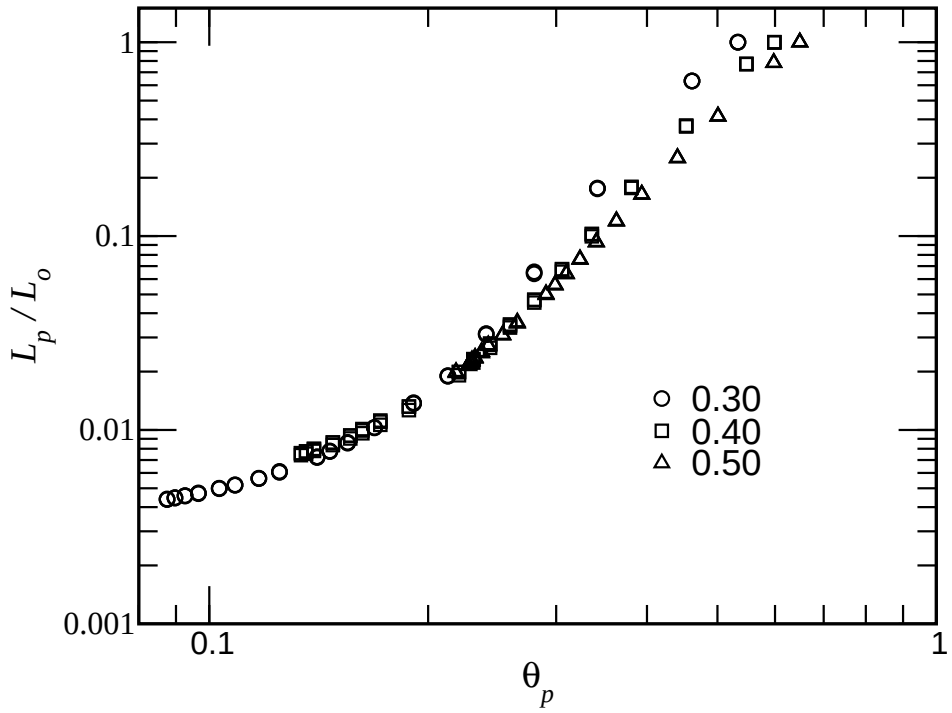

Figure 5: Paste transport factor L_p, divided by the initial value L_o as a function of paste capillary porosity θ_p for the three w/c values.

Table 2: Degree of hydration at the time of cracking for the three w/c values.

w/c	3.5 d	33 d
0.30	0.49	0.64
0.40	0.53	0.79
0.50	0.58	0.82

7 Cracked Paste Properties

The results that follow are from systems having a crack width of either 2 μm, 4 μm, 8 μm, 16 μm, or 32 μm. The cracks were initiated either at 3.5 d or 33 d of model hydration. The degree of hydration of each paste at the time of cracking is shown in Table 2. To facilitate the analysis, the results for the systems cracked at 3.5 d are presented first. An analysis of the systems cracked at 33 d is made in context of the methods used to study the systems cracked at 3.5 d.

As a convenient shorthand, variables having subscripts denote time-dependent quantities, and variables with superscripts denote constants.

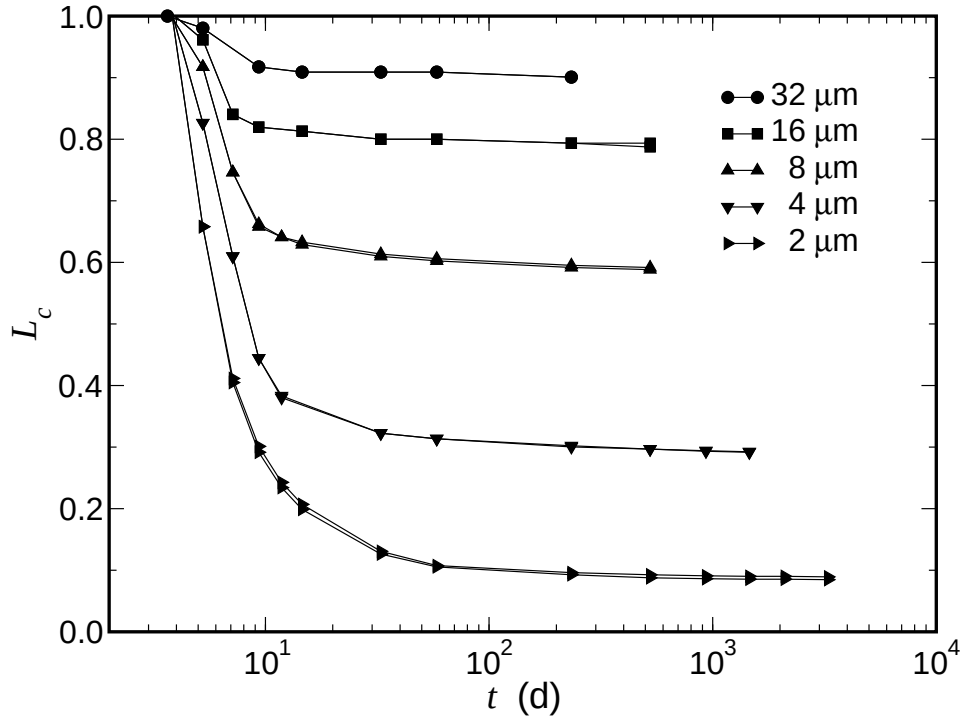

Figure 6: Crack transport factor L_c as a function of time t for different crack widths in 0.30 w/c paste.

7.1 Transport Factor vs. Time

For each w/c value and crack width, the crack transport factor L_c is plotted as a function of time in Figs. 6–8. Both values for L_c at each point are plotted in the figures, but often the two values nearly coincide. For a given w/c value, the transport factors of narrower cracks decrease more rapidly and reach a lower ultimate value than those for wider cracks. This trend is expected intuitively because less solid material is required to fill a narrower crack.

Taken all at once, establishing a consistent picture of crack healing would be a daunting task. Instead, the problem is broken into two separate tasks: determine how the crack transport factor depends upon crack porosity; and determine the factors that control the rate that the porosity within the crack is filled with material.

7.2 Transport Factor vs. Porosity

Based on the transport factor calculations for the uncracked paste discussed previously, there may be a universal relationship between crack transport factor and crack porosity. For cracks, however, there is no need to divide the crack transport factor by its initial value because the initial value is one. The crack transport factor L_c for the systems cracked at 3.5 d are shown in Fig. 9 as a function of the crack porosity θ_c. As can be seen in the figure, there appears to be a universal relationship between crack porosity and crack transport factor, independent of crack width and cement paste w/c value.

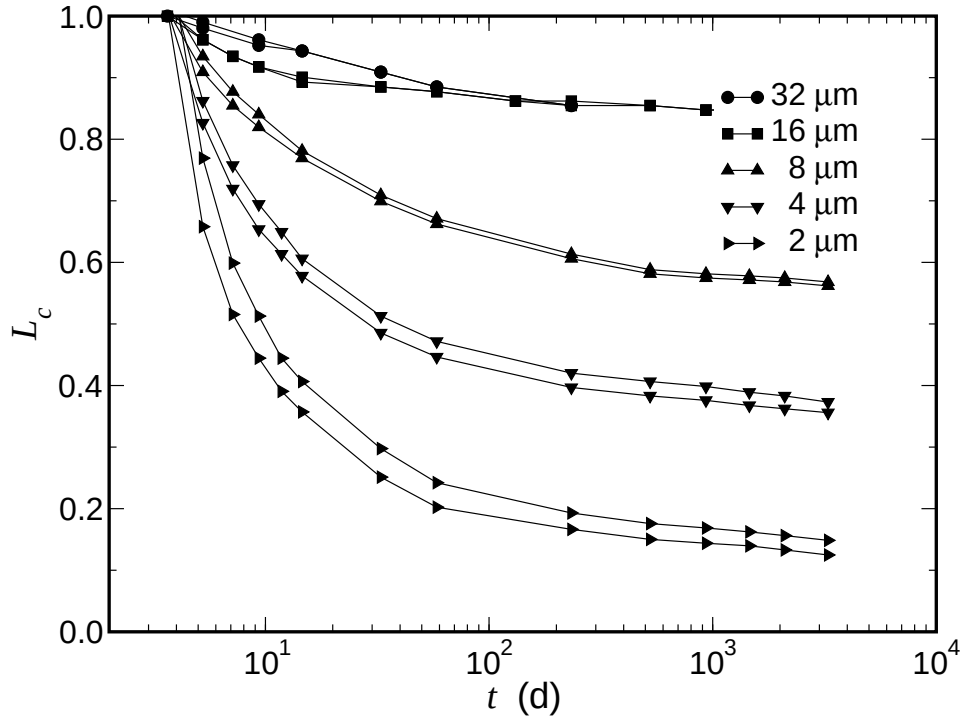

Figure 7: Crack transport factor L_c as a function of time t for different crack widths in 0.40 w/c paste.

The data plotted in Fig. 9 suggests that there might exist a critical crack porosity, below which the transport factor L_c is zero. To corroborate this hypothesis, the data in Fig. 9 are plotted again in Fig. 10 as a function of a reduced crack porosity Θ_c:

$$\Theta_c = \frac{(\theta_c - \theta^{crit})}{(1 - \theta^{crit})} \tag{10}$$

A log-log plot of the data, using a critical porosity θ^{crit} equal to 0.35, yields a reasonably straight line with slope near 1.5. This is used as an approximation for the crack transport factor L_c:

$$L_c = \Theta_c^{3/2} \tag{11}$$

The function $\Theta_c^{3/2}$ is shown as a solid line in Fig. 10, and appears to characterize all the data.

A value of 0.35 for the critical porosity θ^{crit} is consistent with results from percolation studies on two-dimensional systems. Studies of the percolation threshold for randomly located overlapping circles have yielded critical porosities ranging from 0.31 to 0.38 [45, 46], while pixel-based representations of circles on a lattice have yielded critical porosities of 0.35 and 0.33 [47], the latter value for higher resolution circles. Similarly, critical porosities for randomly located overlapping squares of a fixed orientation have ranged from 0.33 to 0.39 [48–50], and the critical value for the same objects on a lattice was 0.35 [47].

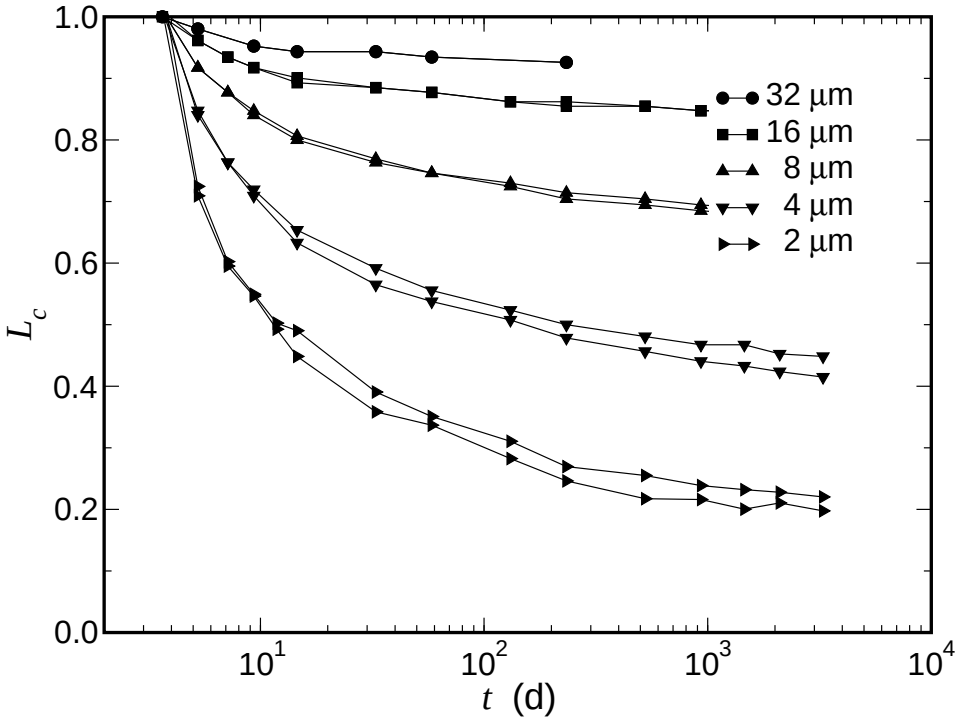

Figure 8: Crack transport factor L_c as a function of time t for different crack widths in 0.50 w/c paste.

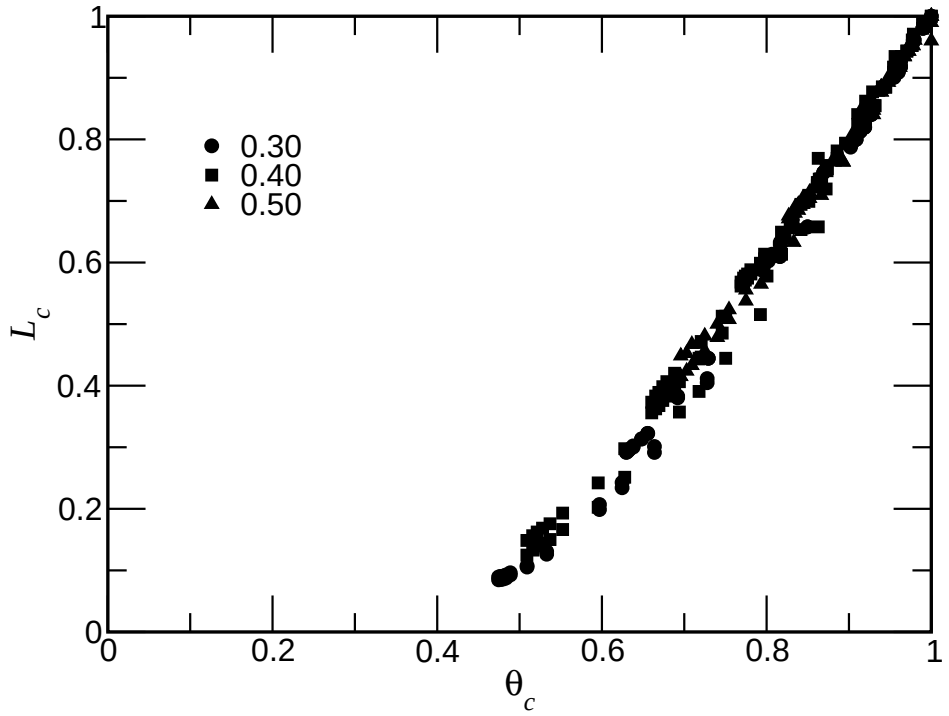

Figure 9: Crack transport factor L_c as a function of the crack porosity θ_c.

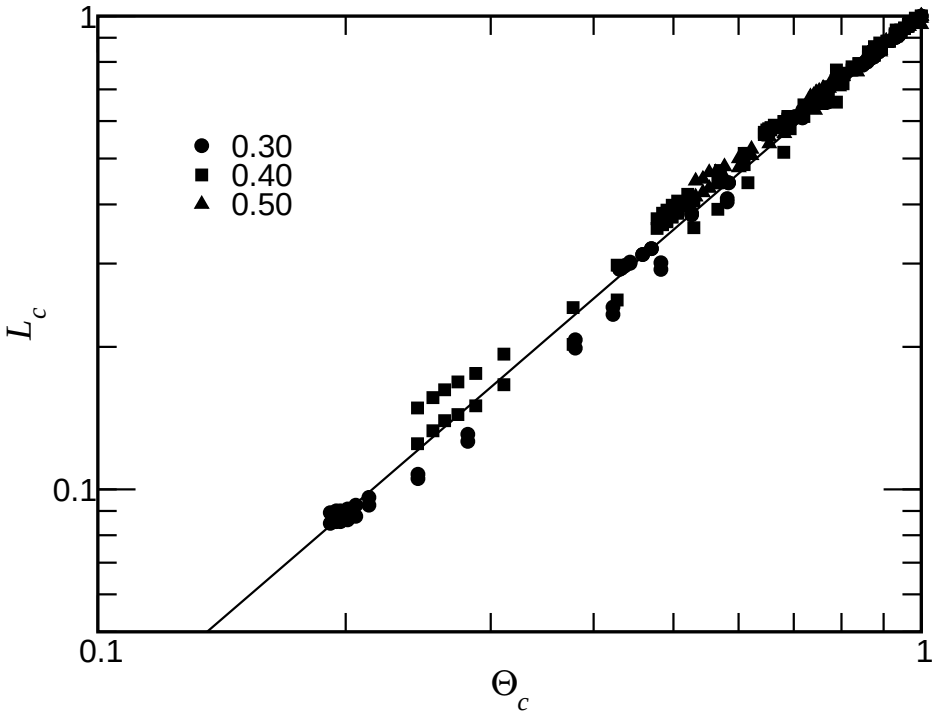

Figure 10: Crack transport factor L_c as a function of the reduced crack porosity Θ_c (see Eqn. 10). Solid line is $\Theta_c^{3/2}$.

Another significance of these results is that these model systems having cracks up to 16 μm wide behave like two-dimensional systems. For wider cracks, one would expect that the microstructure within the crack will have a three-dimensional structure. As such, these cracks would have a lower critical porosity at percolation. Therefore, the transport properties of wider cracks would be greater, at the same porosity, that narrower cracks.

The relationship between crack transport factor and crack porosity in the systems cracked at 33 d were sufficiently similar to the systems cracked at 3.5 d that presenting the data would be redundant.

7.3 Crack Solids Production

Given the apparent universal relationship between crack porosity and crack transport factor, the remaining challenge is to determine the time required for a crack to achieve a given porosity. Crack porosity θ_c for a 2-μm, a 4-μm, and an 8-μm crack initiated at 3.5 d is shown in Fig. 11 as a function of time for all three w/c values. Cracks in lower w/c pastes fill faster, as has been observed experimentally [5]. In seeming contradiction, the ultimate crack porosity appears to be lower for higher w/c pastes. Note that the porosity of the 8 μm cracks in the 0.40 w/c paste falls below the porosity of the corresponding 0.30 w/c paste.

Given these two observations, one can develop a conceptual model for crack filling. The fact that lower w/c pastes fill cracks faster initially means that transport of hydration

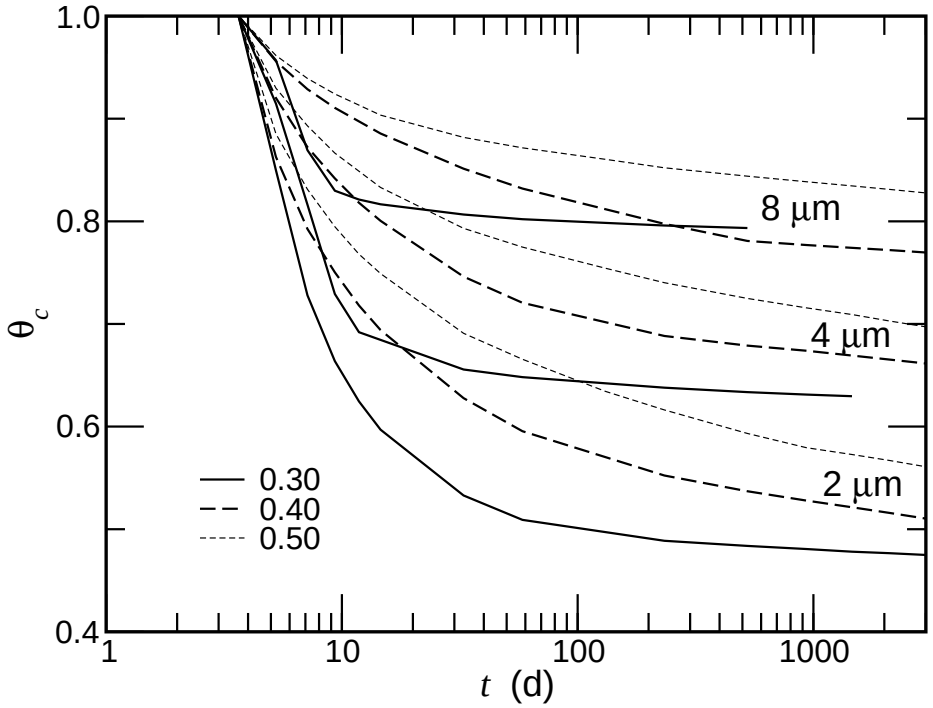

Figure 11: Crack porosity θ_c as a function of time t for 2 μm, 4 μm, and 8 μm cracks initiated at 3.5 d.

product from the paste to the crack is not a primary mechanism because the paste transport factor is considerably smaller for lower w/c pastes. Therefore, crack filling at early times is probably due to hydration product formed in close proximity of the crack. At later times, there is a slower crack filling mechanism that seems to favor higher w/c pastes. This behavior is consistent with leaching of soluble materials in proximity to the crack. Higher w/c pastes have a greater percentage of portlandite in the pores, and the higher transport coefficients contribute to additional transport.

7.4 Leaching

The solids within the crack must originate from either hydration of cement elements at or near the crack wall, or from solids in the paste that dissolve and then precipitate in the crack (i.e., leaching). Although the microstructural model does not individually label solids of similar composition, it is still possible to determine what fraction of the solid elements within the crack originated from the bulk paste. If the crack had no influence on microstructural development within the bulk paste, the microstructure on either side of the crack would remain identical to the microstructure of the corresponding uncracked system. By contrast, any differences between the cracked and uncracked systems in the bulk paste, particularly the porosity, must be an effect of the crack.

One effect of the crack will be to redistribute portlandite from the paste to the crack, in a manner similar to leaching. Figure 12 shows the volumetric ratio of portlandite

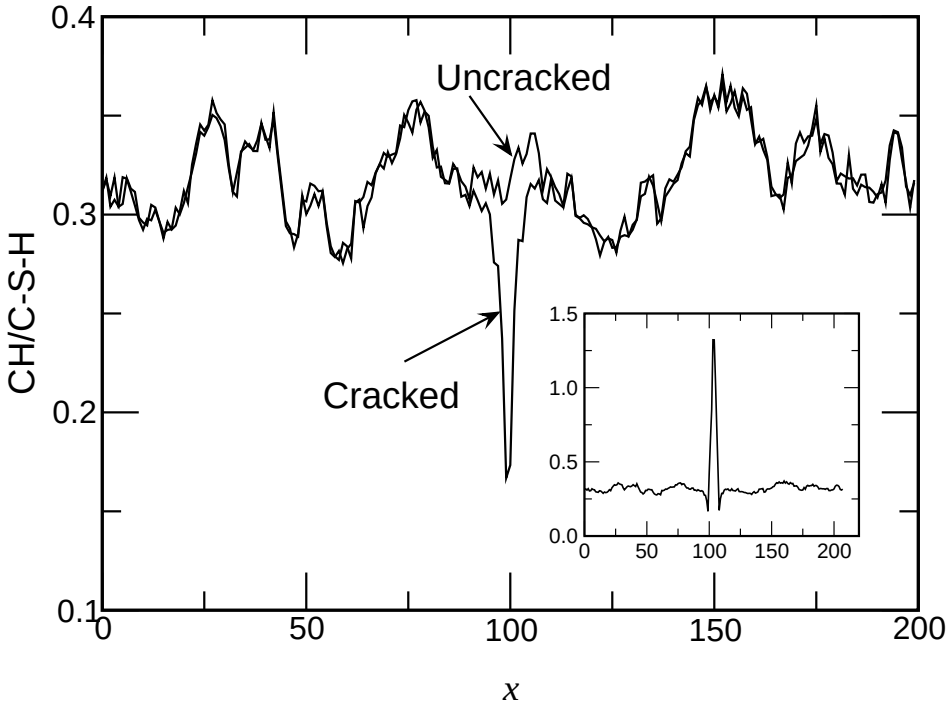

Figure 12: Ratio of portlandite (CH) to C-S-H in the 0.5 w/c systems at 10,000 cycles, after developing an 8 μm crack at 500 cycles. Distance x represents slices parallel to the crack that is located at $x = 100$; see text for additional explanation. Inset shows the same ratio for the cracked system, including the crack.

(CH) to C-S-H, calculated from the voxels in the 200×200 planes parallel to the crack. The system is the 0.5 w/c paste after 10,000 cycles, with a 8 μm crack appearing after 500 cycles. The main plot shows both the cracked and uncracked systems, with the crack being omitted. The inset graph shows the ratio for the cracked system, including the crack. Far away from the crack, the CH/C-S-H ratios are nearly equal for both systems. In the paste near the crack the ratio decreases, and inside the crack the ratio is considerably higher than that for the paste. These two effects are consistent with CH leaching from the paste and precipitating inside the crack.

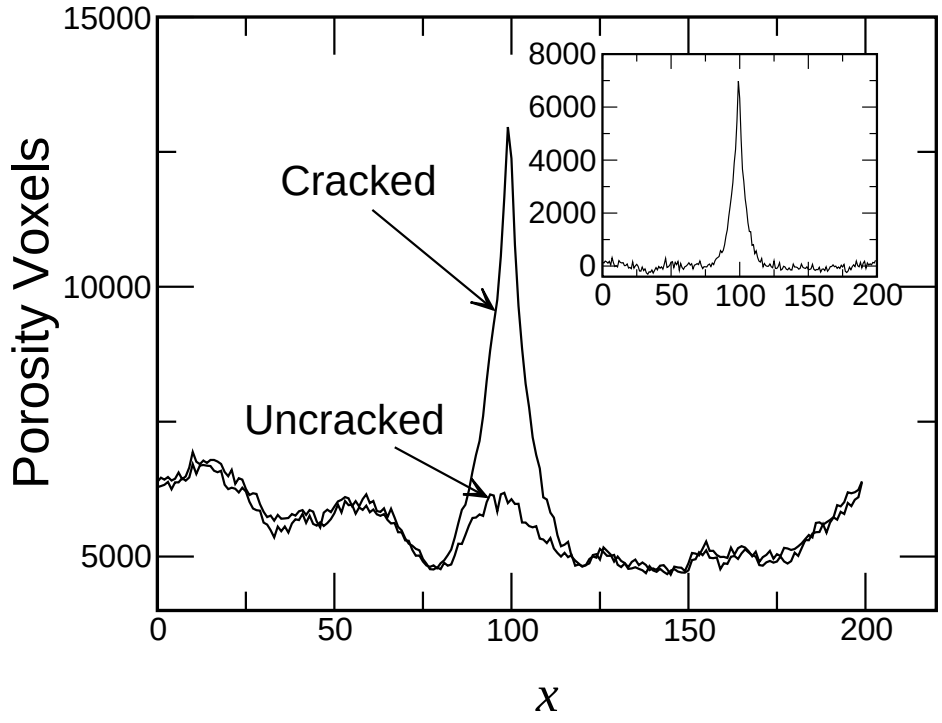

Figure 13: Porosity voxels of cracked (8 μm at 500 cycles) and uncracked 0.40 w/c systems at 10 000 cycles hydration. Distance x represents slices parallel to the crack that is located at $x = 100$; see text for additional explanation. Inset shows the difference between the two curves.

Other soluble species in the model would also be undergoing the same phenomenon, leading to an overall increase in the paste porosity in proximity to the crack. Figure 13 shows the number of porosity pixels in each 200×200 plane parallel to the crack; the crack planes have been omitted from the comparison. The data in the figure demonstrate that the number of porosity pixels in the paste is nearly the same for both the cracked and uncracked microstructures, except within approximately 15 μm of the crack, where the porosity in the cracked system increases. The difference in the two curves in Fig. 13 is shown in the inset. Therefore, not only are voxels of soluble material leaching from the paste, they are leaving behind regions of higher porosity just outside the crack.

The total number of porosity pixels in a plane P is calculated for both the cracked (P_c) and uncracked systems (P_o). The difference ($P_c - P_o$) is plotted in Fig. 14 for the

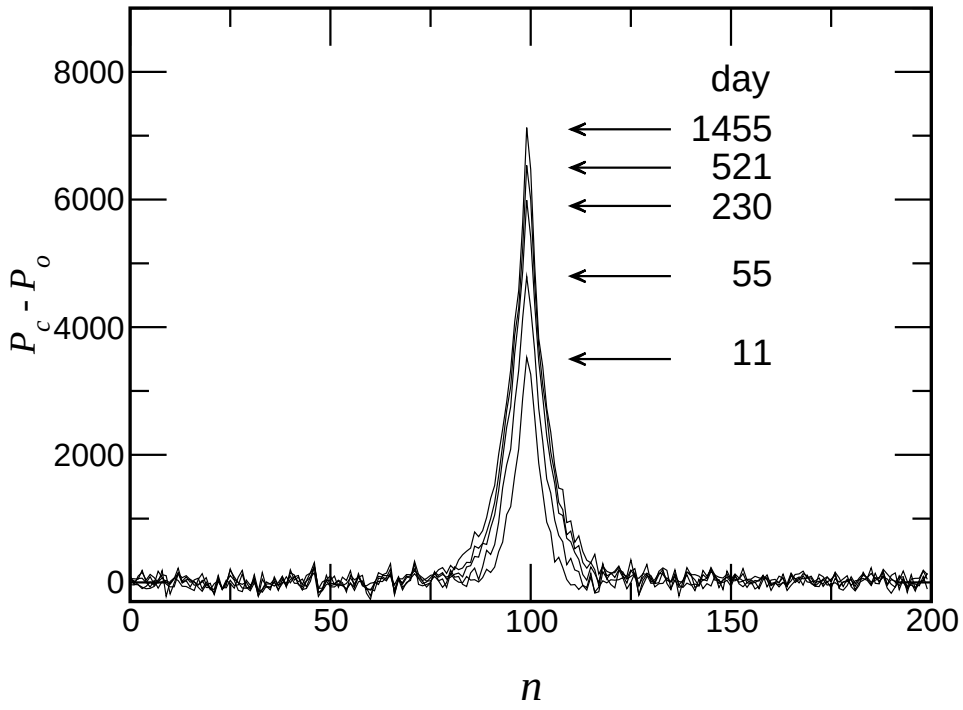

Figure 14: Leached bulk paste porosity in 0.4 w/c paste having a 8 μm crack initiated at 3.6 d. Numbers indicate elapsed days after crack formed.

0.4 w/c paste having a crack of width 8 μm. The numbers in the figure denote the elapsed time in days since cracking first occurred. Because the degree of hydration of the cracked systems was always within 2 % of that for the uncracked system, the paste portion of these systems after the same number of cycles should be nearly identical. The data show random fluctuations about zero for the paste farthest from the crack, and a dramatic increase in the number of porosity pixels in proximity to the crack.

The sum of $(P_c - P_o)$ represents the total number of solid elements missing from the paste portion of the cracked system. Because these calculations are made on a closed system, these solid elements could only have diffused into the crack. If Σ_p represents the sum of $(P_c - P_o)$, and S_c represents the number of solid elements in the crack, the ratio Σ_p/S_c represents the fraction of solids in the crack that can be accounted for by leaching from the paste. Here, this ratio will be referred to as the leaching index Λ.

The leaching index Λ for the 0.40 w/c and the 0.50 w/c cement pastes are shown in Fig. 15. The data for the 0.40 w/c system includes only the systems cracked at 3.5 d, while the data for the 0.50 w/c system includes data for both the 3.5 d cracking and the 33 d cracking. Difficulties in how CEMHYD3D handles systems with very low porosity prohibited a quantitative analysis of the 0.30 w/c systems. The results for the 0.40 w/c and 0.50 w/c pastes indicate that the majority of solids in the crack can be attributed to leaching from the bulk cement paste, regardless of when cracking occurs.

Although the effect of the crack is to leach portlandite from the surrounding paste, the mechanism of leaching in the microstructural model is not physically accurate. There

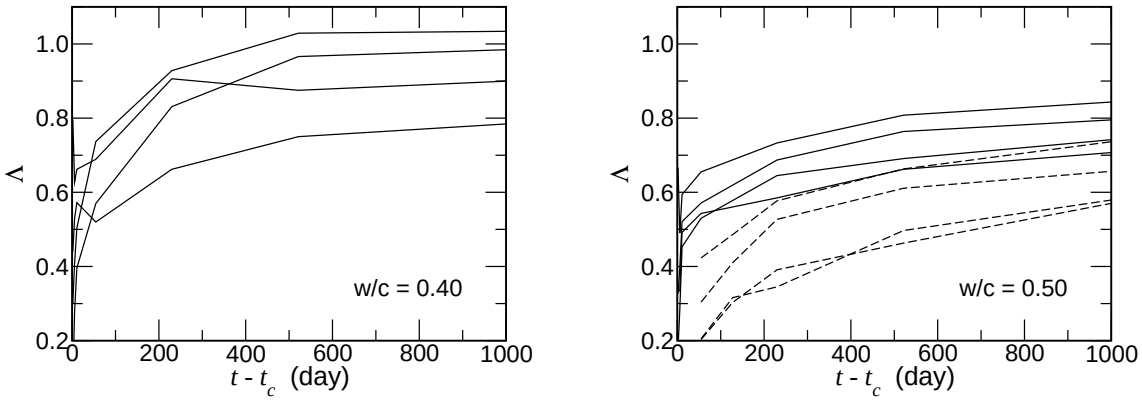

Figure 15: Leaching index Λ as a function of the time t after cracking occurs at t_c in systems having w/c = 0.4 and 0.5. The solid lines denote data for cracks initiated at 3.6 d, and dashed lines denote data for cracks initiated at 33 d.

is no rigorous model for transport within the model. Rather, there is dissolution of portlandite, and the portlandite "diffuses" as a solid species that has some probability of precipitating. This is true for all the soluble minerals in the model. Therefore, the amount of leaching is related to other microstructural development parameters like the degree of hydration.

7.5 Crack Solids vs. Time: Early Age

Both the volume of hydration product formed and the volume of soluble materials leached into the crack should be (nearly) independent of the crack width. Therefore, the total volume of solids within a crack, at a given time, should be independent of crack width. The volume of hydration product that can be formed after cracking occurs depends upon the difference between the degree of hydration at the time of cracking and the maximum degree of hydration. Moreover, this same difference characterizes the amount of materials that can be leached from the cement paste.

To test this assertion, the crack solids content, expressed as the product of crack width w and crack solids fraction $\phi_c = (1 - \theta_c)$, is plotted in Fig. 16 as a function of the difference between the paste degree of hydration α_p and the degree of hydration at the time of crack initiation α^i (see Table 2). The dotted and dashed curves are labeled, and the solid lines correspond to 16 μm and 32 μm cracks. The solid straight line passes through the origin and has a slope of 5. Although, for a given w/c paste, the curves for all the crack widths do not lie upon one another, the curves for the wider crack widths are in proximity to one another. Given the discrete nature of the CEMHYD3D model, the deviations for narrower cracks are attributed to finite-size effects.

It is interesting to note that both the 0.30 w/c and the 0.40 w/c paste curves in Fig. 16 diverge above the straight line, while the 0.50 w/c curve diverges below the straight line. A common distinction between these two groups is that the 0.30 w/c and the 0.40 w/c pastes experience a de-percolation of the capillary porosity during the calculation. The amount of hydration after cracking ($\alpha_p - \alpha^i$) at which this occurs is shown in Fig. 16 as

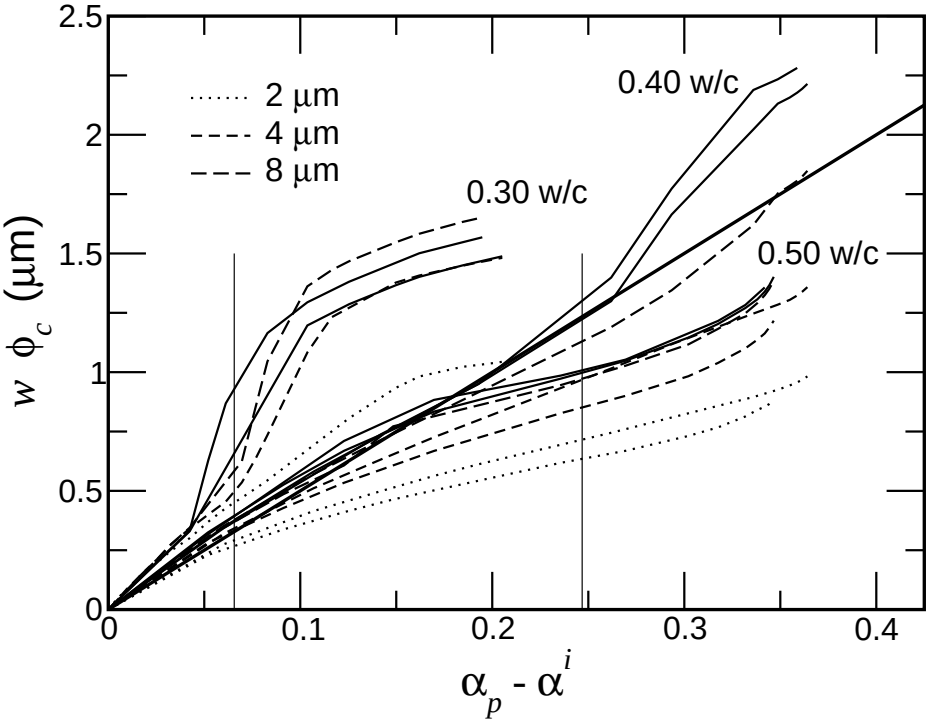

Figure 16: Crack solids content for systems crack at 3.5 d, expressed as a function of crack width w and crack solids fraction ϕ_c, as a function of the degree of hydration α_p occurring after the the degree of hydration at the time of cracking α^i. The solid lines correspond to 16 μm and 32 μm cracks. The left and right vertical lines correspond to when the 0.30 w/c paste and the 0.40 w/c paste de-percolate, respectively. The straight line is $5(\alpha_p - \alpha^i)$.

the two vertical lines. The divergence of the 0.30 w/c and the 0.40 w/c pastes from the straight line occurs near the time at which the capillary pores are no longer percolated, which suggests that the de-percolation of capillary porosity causes the diverging behavior.

7.6 Crack Solids vs. Time: Late Cracking

A similar analysis was performed for the systems cracked at 33 d, and the data are shown in Fig. 17. The straight line in the figure has a slope equal to that shown in Fig. 16. Although the relationship between crack solids content and degree of hydration after cracking eventually become somewhat linear with similar slopes as for the systems cracked at 3.5 d, there is a period immediately after cracking during which the filling mechanism is noticeably different, as is apparent by the different initial slopes for the different w/c values. This different behavior is likely due to a crack filling mechanism that has not yet been discussed.

At 33 d, each system already has hydrated to more than 88 % of its ultimate degree of hydration. Therefore, when a crack forms at this age, the contribution of continued bulk hydration must be significantly less than that for the systems cracked at 3.5 d.

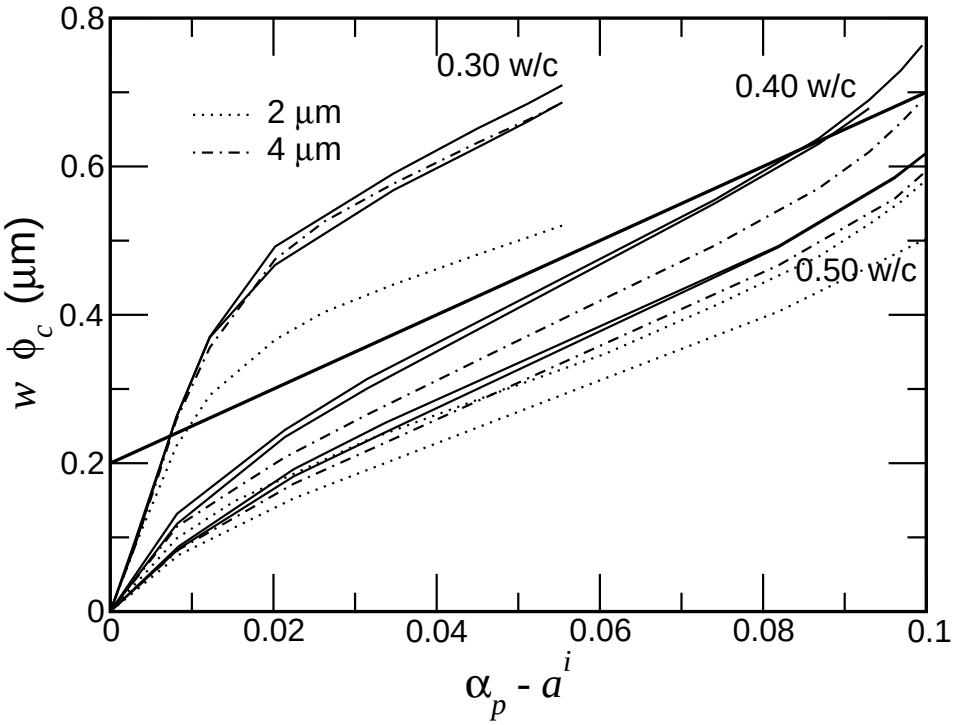

Figure 17: Crack solids volume $w\phi_c$ for systems cracked at 33 d, expressed as a function of the degree of hydration α_p occuring beyond the degree of hydration at cracking α^i. Solid line intersecting the ordinate axis at 0.2 has same slope as the line in Fig. 16.

By comparison to Fig. 16, when cracks form in older pastes, less hydration occurs and considerably less hydration product is formed in the crack. This has been observed experimentally [9].

Table 3: Crack wall area fraction of unhydrated clinker A^w. The second number is the expected value calculated from product of the initial solids fraction and the degree of hydration at the time of cracking.

w/c	3.5 d	33 d
0.30	0.229/0.238	0.151/0.168
0.40	0.172/0.190	0.066/0.085
0.50	0.140/0.147	0.054/0.064

Based on the model used here, the process of creating cracks exposed unhydrated clinker at the crack wall. This sudden exposure to unhydrated clinker could, at these late ages, contribute significantly to the volume of crack solids. Table 3 shows the crack wall area fraction of unhydrated clinker A^w, along with an estimate of the same quantity based on the initial cement volume fraction and the degree of hydration at the time of cracking. In general, the two values agree with one another.

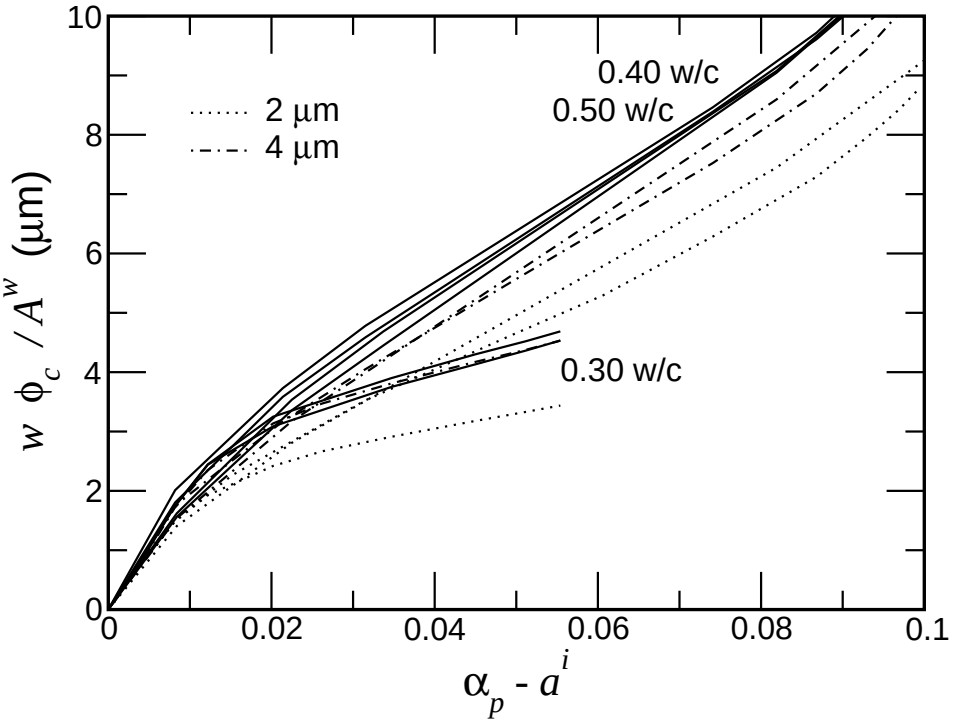

Figure 18: Crack solids content $w\phi_c$, divided by the crack wall area fraction of unhydrated clinker A^w as a function of continued hydration ($\alpha_p - \alpha^i$).

Given the advanced degree of hydration for the systems cracked at 33 d, it may be possible for the exposed unhydrated clinker on the crack wall to contribute significantly to the initial rate of crack filling. Based on this hypothesis, the crack solids volume $w\phi_c$, divided by the crack wall area fraction of clinker A^w, is plotted as a function of the degree of hydration after cracking, and is shown in Fig. 18 for all three w/c values. The co-linearity near the origin among the different w/c values suggests that crack surface hydration may indeed play an important role in the initial rate of crack filling when cracks appear at late ages.

7.7 Crack Surface Hydration

Because CEMHYD3D is a discrete model, the contribution of crack wall surface hydration can be, to a certain extent, extracted from the degree of hydration of the cracked system α_b. As the cracked system hydrates, the rate of hydration will be slightly greater than that for the uncracked system. The difference could be both from crack surface cement hydration and from additional hydration in the bulk due to the presence of the water in the crack. Although the individual hydration sites were not monitored during the calculation, it may be possible to make some general inferences based on knowing the number of crack surface cement elements.

In CEMHYD3D, the degree of hydration is calculated from the number of volume elements of cement remaining at any given moment. Therefore, at the time of crack

formation, there exists a number of cement elements on the crack surface. The ratio of the number of cement elements on the crack surface to the total number of cement elements initially corresponds to the contribution to the overall degree of hydration attributed to hydration of the first layer of cement element on the crack surface α^w.

To quantify the contribution of crack wall hydration, it is compared to the difference between the degree of hydration in the cracked system α_b and the degree of hydration in the uncracked paste α_p. This difference, divided by the potential contribution to crack surface hydration α^w, would correspond to the equivalent number of crack surface layers that would have to hydrate to account for the difference.

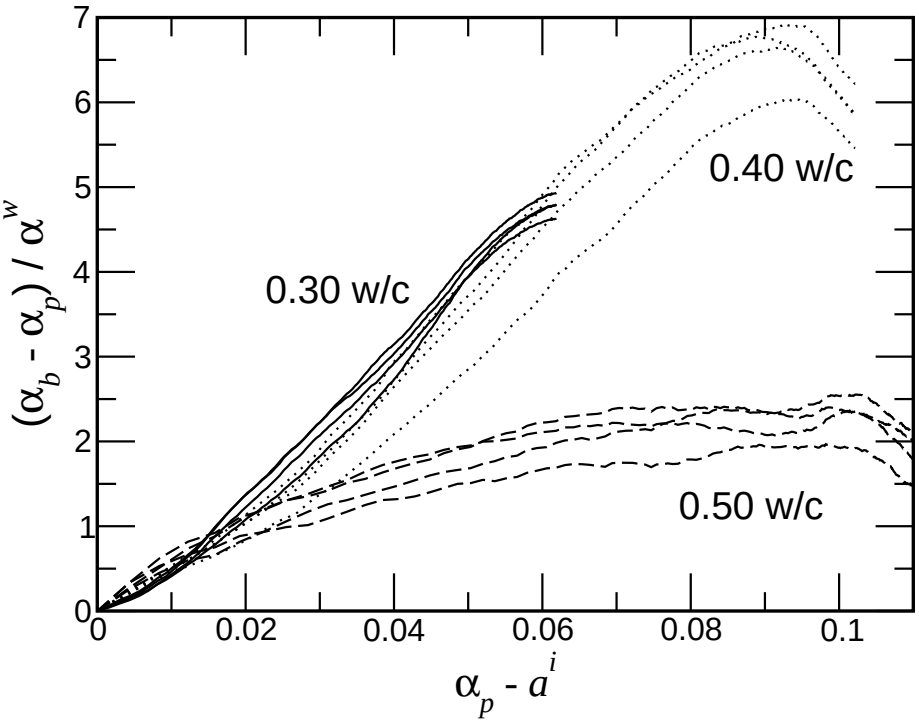

Figure 19: The fraction of the difference between the degree of hydration in the cracked system α_b and that of the uncracked system α_p, relative to the contribution α^w of the clinker exposed at the crack walls.

These data are shown in Fig. 19 for the systems cracked at 33 d. As can be seen in the figure, one equivalent layer of crack surface cement elements has hydrated after $(\alpha_p - \alpha^i) = 0.02$ for all three w/c values. Interestingly, the same value for $(\alpha_p - \alpha^i)$ in Fig. 18 is near the transition between the initial production mechanism (initial slopes) and the final production mechanism (final slopes).

8 Discussion

Although one cannot state definitively the exact crack healing behavior of all cement pastes based on this model study, one should be able to argue for general relationships

and for principle components (i.e., those physical parameters having the greatest influence on a result).

8.1 Healing Capacity: Early Cracking

For systems developing cracks at early ages, the minimum crack porosity achievable depends upon the degree of hydration at the time of cracking, along with the maximum degree of hydration. Based on data shown in Fig. 16, the difference between the maximum degree of hydration α^{max} and the degree of hydration at the time of cracking α^{i} determines the maximum solids content of a crack.

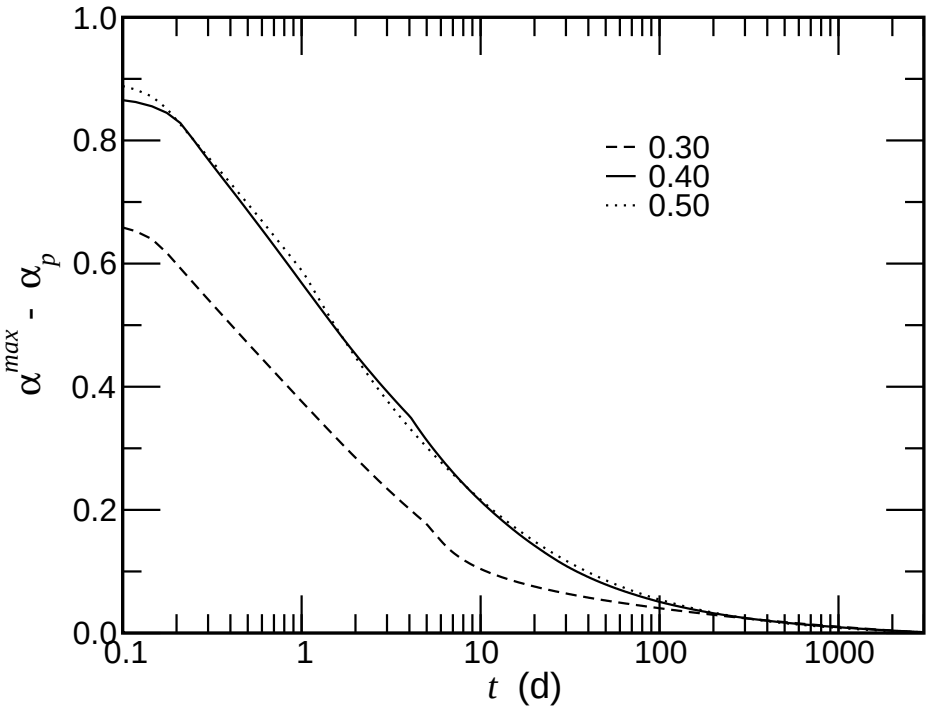

Figure 20: Difference between maximum degree of hydration α^{max} and the time-dependent degree of hydration α_p as a function of time t.

A plot of $(\alpha^{max} - \alpha_p)$ is shown in Fig. 20 for all three w/c values. This plot is a measure of the healing capacity of a crack, when cracks occur at early ages. Generally, higher w/c value pastes have a greater capacity to fill in cracks of a given width. Based on the curves for the 0.40 w/c and 0.50 w/c pastes, however, the capacity appears to saturate because of the competition between rate of hydration and maximum degree of hydration α^{max}.

8.2 Healing Capacity: Late Age

At later ages, the volume fraction of unhydrated clinker may play a role in crack filling, which suggests an alternative interpretation of late age healing capacity. The volume

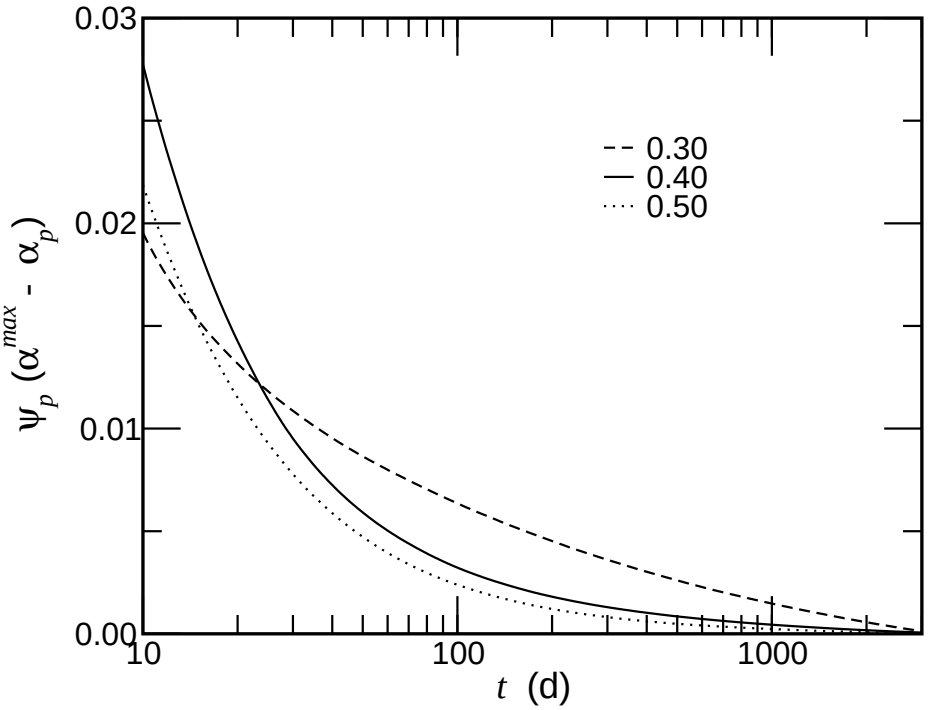

Figure 21: Difference between maximum degree of hydration α^{max} and the paste degree of hydration α_p, times the volume fraction of unhydrated clinker in the paste ψ_p (see Eqn. 12), as a function of time t.

fraction of unhydrated clinker in the paste ψ_p depends on the paste degree of hydration α_p and the initial volume fraction of cement in the paste ψ_p°:

$$\psi_p = \psi_p^\circ \, (1 - \alpha_p) \tag{12}$$

The product $\psi_p(\alpha^{max} - \alpha_p)$ is plotted in Fig. 21 as a function of time for the three w/c values. Based on this definition of healing capacity, low w/c pastes should heal better when cracking occurs at late ages.

The validity of this definition of healing capacity, suggesting that 0.4 w/c pastes should perform better for early cracking, is partially supported by Fig. 11. Although initially the porosity decreases fastest for the 0.3 w/c paste, it appears that the porosity of the corresponding 0.4 w/c and 0.5 w/c pastes eventually fall below that of the 0.3 w/c paste. For increasing crack width, however, the porosity of the 0.40 w/c paste fell below that of the 0.30 w/c paste much sooner than the 0.50 w/c paste. Therefore, although the 0.40 w/c and the 0.50 w/c pastes should have roughly the same healing capacity for early cracks, the presence of more unhydrated clinker in the 0.40 w/c paste has the practical effect of speeding the recovery of the 0.40 w/c paste over that of the 0.50 w/c paste. These results suggest that if cracks are anticipated at early age, a moderate w/c is best, and if cracks are anticipated at later ages, a lower w/c is best.

8.3 Crack Permeability

The relationship between crack transport factor and crack porosity given in Eqn. 11 can be substituted into the general expression for the permeability of pseudo two-dimensional structures given in Eqn. 6 to yield an approximation for the permeability of a crack k_c as a function of the crack initial width w and porosity θ_c:

$$k_c = \theta_c^4 \left(\frac{\theta_c - 0.35}{1 - 0.35}\right)^{3/2} \frac{w^2}{12} \tag{13}$$

Based on the observed data, a crack porosity of 0.5 appears to be lower bound on hydration-induced crack healing. At this porosity, Eqn. 13 predicts the crack permeability would decrease to approximately 1/144 of its initial value. If the formation of the cracks increased the overall permeability by a factor of γ, reducing the crack porosity to 50 % would reduce the overall permeability to approximately $\gamma/144$. Therefore, one would see approximately a two order of magnitude decrease in the overall permeability. Of course, this minimum porosity could only be achieved in the smallest cracks.

8.4 Wide Cracks

The widths of cracks used in this study were limited by experimental constraints. The 200^3 system is near the practical limit of existing computational resources. Given this dimensional constraint, cracks that are wider than 32 μm would consume a significant fraction of the total volume and would contribute to a majority of the total system porosity. Regardless, the data suggest that calculations using wider cracks would not contribute significantly to the understanding of continued hydration on crack healing.

By observation of the results in this study, and by extrapolation, one could conclude that cracks that are significantly wider than approximately 10 μm will probably not heal much, if at all, due to continued hydration alone. Under the most ideal conditions of early cracking in a 0.4 w/c paste, Fig. 16 suggests an upper bound for $w\phi_c$ to be approximately 2.5 μm. For the case of a 100 μm crack, the maximum crack solids fraction would be 2.5 %, or 97.5 % porosity. Using Eqn. 13, the hydration product would reduce the crack permeability to 85 % of the water-filled crack permeability. It is likely that this change would be within experimental uncertainty, and the one might conclude that healing is insignificant, or nonexistent, in cracks wider than 100 μm. This conclusion is consistent with experimental observations of a diminishing number of crack filling "bridges" as the crack width approaches 10 μm [23]. In field concrete, however, other mechanisms can contribute to the filling of wider cracks, but they may be more difficult to quantify.

8.5 Clinker Aggregates

Some of the inferences made from this experiment are predicated on the expectation that a crack forming in the paste content of a concrete will expose surfaces of unhydrated cement. This generally should happen if the cohesive strength of the C-S-H is greater than either the cohesive strength of the unhydrated material or the adhesive strength of the interface between C-S-H and the unhydrated cement particles on which it forms.

However, in the absence of fresh cement surface being exposed at newly-formed crack walls, the effect of the unhydrated clinker volume on late-age crack healing could be practically non-existent.

One could, in some applications, improve the chances of exposing unhydrated cement by using clinker or coarsely ground cement as a component of the aggregates. The use of clinker as aggregate has been proposed previously [51], but not for application to crack healing. As shown in Fig. 1, cracks propagate through unhydrated cement. Therefore, cracks should propagate through more coarsely ground cement because they still have the defects that grinding eliminates. Although the addition of clinker aggregate would improve the overall crack healing performance for any w/c paste, based on the results presented here, the right formulation of clinker aggregate in a 0.40 w/c mixture could have superior performance at all ages of cracking.

8.6 NDE Significance

A unique relationship between crack transport factor and crack porosity, as suggested by the data in Fig. 9, would have a very practical significance for crack characterization in the field. In general, the three crack parameters that have the greatest influence on overall transport, in decreasing order of significance, are crack depth, crack transport coefficient, and crack width. The first two can effect bulk transport properties by orders of magnitude. For fixed crack depth and crack transport coefficient, however, the total transport through the crack is only linearly dependent on the crack width.

Fig. 9 suggests that determining crack porosity is sufficient for characterizing the crack transport coefficient, regardless of the crack width. Given corroborating evidence, it would suggest that NDE research on characterizing cracks could achieve great gains by developing the ability to estimate crack porosity.

9 Summary

A microstructural model can be a useful investigatory tool for evaluating the principal components having the greatest effect on the healing of cracks through continued hydration. Results indicate that the transport property of a crack depends largely on the crack porosity, independent of initial crack width or cement paste w/c value. This result is consistent with the premise that the mechanism by which the cracks fill is independent of crack width and cement paste w/c. This result is significant for future investigations attempting to characterize cracks using non-destructive evaluation (NDE) techniques.

Further analysis of the results suggests that the mechanism by which the cracks heal has two components. The initial rate of healing depends upon the amount of unhydrated cement exposed at the time of cracking. These hydration reactions lead to a rapid production of hydration products within the crack. The initial hydration of exposed unhydrated cement is quickly exhausted, and the remainder of the crack filling depends upon redistribution of hydration product from the bulk paste. For cracking occurring at early ages, the contribution to crack filling from the hydration of exposed unhydrated clinker is very small. At later ages, however, the contribution of exposed unhydrated

clinker can become comparable to that of continued hydration. This result led to the speculation of the advantage of using clinker fine aggregate to mitigate the effect of cracking at late ages.

Acknowledgements

The authors would like to thank Paul Stutzman (National Institute of Standards and Technology) for providing the SEM micrograph in Fig. 1.

References

[1] N. Hearn and C. T. Morley. Self-sealing property of concrete - Experimental evidence. *Mater. Struct.*, 30:404–411, 1997.

[2] N. Hearn. Self-sealing, autogenous healing and continued hydration: What is the difference? *Mater. Struct.*, 31:563–567, 1998.

[3] S. Jacobsen, J. Marchand, and B. Gérard. Concrete cracks I: Durability and self healing – A review. In O. E. Gjørv, K. Sakai, and N. Banthia, editors, *Concrete Under Severe Conditions 2*, volume One, pages 217–231. E& FN Spon, 1998.

[4] C. Edvardsen. Water permeability and autogenous healing of cracks in concrete. *ACI Mater. J.*, 96(4):448–454, 1999.

[5] C. A. Clear. The effects of autogeneous healing upon the leakage of water through cracks in concrete. Technical report, Cement and Concrete Association, Slough, UK, 1985.

[6] L. Turner. The autogeneous healing of cement and concrete: Its relation to vibrated concrete and cracked concrete. Technical report, International Association for Testing Materials, April 1937.

[7] S. Jacobsen, H. C. Gran, E. J. Sellevold, and J. A. Bakke. High strength concrete – Freeze/thaw testing and cracking. *Cem. Concr. Res.*, 25:1775–1780, 1995.

[8] S. Jacobsen, J. Marchand, and H. Hornain. SEM observations of the microstructure of frost deteriorated and self-healed concretes. *Cem. Concr. Res.*, 25:1781–1790, 1995.

[9] S. Jacobsen and E. Sellevold. Self healing of high strength concrete after deterioration by freezing and thawing. *Cem. Concr. Res.*, 26:55–62, 1996.

[10] S. Jacobsen, E. J. Sellevold, and S. Matala. Frost durability of high strength concrete: Effect of internal cracking on ice formation. *Cem. Concr. Res.*, 26:919–931, 1996.

[11] Y. Abdel-Jawad and R. Haddad. Effect of early overloading of concrete on strength at later ages. *Cem. Concr. Res.*, 22:927–936, 1992.

[12] K. A. Snyder, J. R. Clifton, and L. I. Knab. Freeze-thaw susceptibility of high performance concrete. *Wiss. Z. Hochsch. Archit. Bauwes. (Weimar)*, 40:139–142, 1994.

[13] C.-M. Aldea, M. Ghandehari, S. P. Shah, and A. Karr. Estimation of water flow through cracked concrete under load. *ACI Mater. J.*, 97:567–575, 2000.

[14] D.P. Bentz. CEMHYD3D: A three-dimensional cement hydration and microstructural development modelling package. version 2.0. NISTIR 6485, U.S. Department of Commerce, April 2000.

[15] D.P. Bentz. Three-dimensional computer simulation of cement hydration and microstructure development. *J. Amer. Ceram. Soc.*, 80(1):3–21, 1997.

[16] E. J. Garboczi and D. P. Bentz. Computer simulation of the diffusivity of cement-based materials. *J. Mater. Sci.*, 27:2083–2092, 1992.

[17] C. Edvardsen. Chloride penetration into cracked concrete. In L.-O. Nilsson and J. P. Ollivier, editors, *Chloride Penetration into Concrete*, pages 243–249. RILEM, 1995.

[18] B. Gérard, D. Breysse, A. Ammouche, O. Houdusse, and O. Didry. Cracking and permeability of concrete under tension. *Mater. Struct.*, 29:141–151, 1996.

[19] K. Wang, D. C. Jansen, S. P. Shah, and A. F. Karr. Permeability study of cracked concrete. *Cem. Concr. Res.*, 27:381–393, 1997.

[20] C.-M. Aldea, S. P. Shah, and A. Karr. Water permeability of cracked high strength concrete. In P.-C. Aïtcin and Y. Delagrave, editors, *International Symposium on High-Performance and Reactive Powder Concretes*, pages 211–225. Université de Sherbrooke, 1998.

[21] B. Gérard, S. Jacobsen, and J. Marchand. Concrete cracks II: Observation and permeability – A review. In O. E. Gjørv, K. Sakai, and N. Banthia, editors, *Concrete Under Severe Conditions 2*, volume One, pages 183–197. E& FN Spon, 1998.

[22] C.-M. Aldea, S. P. Shah, and A. Karr. Permeability of cracked concrete. *Mater. Struct.*, 32:370–376, 1999.

[23] S. Jacobsen, J. Marchand, and L. Boisvert. Effect of cracking and healing on chloride transport in OPC concrete. *Cem. Concr. Res.*, 26:869–881, 1996.

[24] B. Gérard and J. Marchand. Influence of cracking on the diffusion properties of cement-based materials Part I: Influence of continuous cracks on the steady-state regime. *Mater. Struct.*, 30:37–43, 2000.

[25] O. G. Rodriguez and R. D. Hooton. Influence of cracks on chloride ingress into concrete. *ACI Mater. J.*, 100:120–126, 2003.

[26] J. Bear and Y. Bachmat. Macroscopic modelling of transport phenomena in porous media. 2: Applications to mass, momentum, and energy transport. *Transport Porous Med.*, 1:241–269, 1986.

[27] K. A. Snyder. The relationship between the formation factor and the diffusion coefficient of porous materials saturated with concentrated electrolytes: theoretical and experimental considerations. *Concr. Sci. Eng.*, 3:216–224, 2001.

[28] K. A. Snyder and J. Marchand. Effect of speciation on the apparent diffusion coefficient in nonreactive porous systems. *Cem. Concr. Res.*, 31:1837–1845, 2001.

[29] A. J. Katz and A. H. Thompson. Quantitative prediction of permeability in porous rocks. *Phys. Rev. B*, 34:8179–8181, 1986.

[30] A. J. Katz and A. H. Thompson. Prediction of rock electrical conductivity from mercury injection measurements. *J. Geophys. Res.*, 92:599–607, 1987.

[31] N. Martys and E. J. Garboczi. Length scales relating the fluid permeability and electrical conductivity in random two-dimensional model porous media. *Phys. Rev. B*, 46:6080–6090, 1992.

[32] L. D. Landau and E. M. Lifshitz. *Fluid Mechanics*. Pergamon Press, second edition, 1987.

[33] N. Hearn, R. D. Hooton, and R. H. Mills. Pore structure and permeability. In P. Klieger and J. F. Lamond, editors, *Significance of Tests and Properties of Concrete and Concrete-Making Materials*, STP 169C, pages 240–262, Philidelphia, PA, 1994. American Society for Testing and Materials.

[34] H. F. W. Taylor. *Cement Chemistry*. Academic Press, 1990.

[35] D.P. Bentz and E.J. Garboczi. Simulation studies of the effects of mineral admixtures on the cement paste-aggregate interfacial zone. *ACI Mater. J.*, 88:518–529, 1991. Available at http://ciks.cbt.nist.gov/monograph/paper23/paper23.html.

[36] D.P. Bentz and S. Remond. Incorporation of fly ash into a 3-d cement hydration microstructure model. NISTIR 6050, U.S. Department of Commerce, August 1997. Available at http://ciks.cbt.nist.gov/∼bentz/flyash/flyash.html.

[37] D.P. Bentz, E.J. Garboczi, C.J. Haecker, and O.M. Jensen. Effects of cement particle size distribution on performance properties of cement-based materials. *Cem. Concr. Res.*, 29:1663–1671, 1999. Available at http://ciks.cbt.nist.gov/∼garbocz/finetwo/paper2col.html.

[38] D.P. Bentz, O.M. Jensen, K.K. Hansen, J.F. Olesen, H. Stang, and C.J. Haecker. Influence of cement particle size distribution on early age autogenous strains and stresses in cement-based materials. *J. Amer. Ceram. Soc.*, 84(1):129–135, 2000. Available at http://ciks.cbt.nist.gov/∼bentz/finedtu/autopsd.html.

[39] C. J. Haecker, D. P. Bentz, X.-P. Feng, and P. E. Stutzman. Prediction of cement physical properties by virtual testing. *Cement International*, 1:86–92, 2003.

[40] R. K. Haupt. Final report: Portland cement proficiency samples number 115 and number 116. Technical report, Cement and Concrete Reference Laboratory, National Institute of Standards and Technology, Gaithersburg, MD, 1995.

[41] E.J. Garboczi. Finite element and finite difference programs for computing the linear electric and elastic properties of digital images of random materials. NISTIR 6269, U.S. Department of Commerce, December 1998. Available at http://ciks.cbt.nist.gov/garbocz/manual/man.html .

[42] K. A. Snyder and D. P. Bentz. Loss of freezable water and cessation of hydration in pastes exposed to 90 % RH. *Cem. Concr. Res.*, 34:2045–2056, 2004.

[43] T. C. Powers, L. E. Copeland, and H. M. Mann. Capillary continuity or discontinuity in cement paste. *PCA Bul.*, (10):2–12, 1959.

[44] E. J. Garboczi and D. P. Bentz. The effect of statistical fluctuation, finite size error, and digital resolution on the phase percolation and transport properties of the nist cement hydration model. *Cem. Concr. Res.*, 31:1501–1514, 2001.

[45] E. T. Gawlinski and H. E. Stanley. Continuum percolation in 2 dimensions - Monte-Carlo tests of scaling and universality for non-interacting disks. *J. Phys. A*, 14:L291–L299, 1981.

[46] T. Vicsek and J. Kertesz. Monte-Carlo renormalization-group approach to percolation on a continuum – Test of universality. *J. Phys. A*, 14:L31–L37, 1981.

[47] E. J. Garboczi, M. F. Thorpe, M. S. DeVries, and A. R. Day. Universal conductivity curve for plane containing random holes. *Phys. Rev. A*, 43:6473–6482, 1991.

[48] M. A. Dubson and J. C. Garland. Measurement of the conductivity exponent in two-dimensional percolating networks - Square lattice versus random-void continuum. *Phys. Rev. B*, 32:7621–7623, 1985.

[49] G. E. Pike and C. H. Seager. Percolation and conductivity: A computer study. I. *Phys. Rev. B*, 10:1421–1434, 1974.

[50] E. T. Gawlinski and S. Redner. Monte-Carlo renormalisation group for continuum percolation with excluded-volume interactions. *J. Phys. A*, 16:1063–1071, 1983.

[51] R. L. Berger. Properties of concrete with cement clinker aggregate. *Cem. Concr. Res.*, 4:99–112, 1974.